Hindawi
Advances in Materials Science and Engineering
Volume 2022, Article ID 6403756, 11 pages
https://doi.org/10.1155/2022/6403756

Research Article

Enhanced Thermoelectric Efficiency of Cement-Based Materials with Cuprous Oxide for Sustainable Buildings

Tao Ji,[1] **Shiping Zhang**,[1] **Yan He**,[2] **Xiong Zhang**,[3] **and Weihua Li**[4]

[1]*School of Architecture and Civil Engineering, Nanjing Institute of Technology, Nanjing 211167, China*
[2]*School of Civil Engineering, Suzhou University of Science and Technology, Suzhou 215011, China*
[3]*School of Materials Science and Engineering, Tongji University, Shanghai 201804, China*
[4]*School of Chemical Engineering and Technology, Sun Yat-sen University, Zhuhai 519082, China*

Correspondence should be addressed to Shiping Zhang; 18018595459@163.com

Received 27 July 2022; Revised 15 September 2022; Accepted 16 September 2022; Published 27 September 2022

Academic Editor: Qian Chen

The thermoelectric effect of plain cement paste is usually weak. To improve the thermoelectric performance of cement composites, functional components, such as carbon fibers, steel fibers, carbon nanotubes, and graphene, are often added to cement paste. In view of the advantage of metal oxides with a higher band gap, pure cuprous oxide crystals with different particle sizes were synthesized by a hydrothermal method and incorporated into the cement matrix to improve the thermoelectric efficiency of cement composites in this study. Pure cuprous oxide crystals with different particle sizes (15 μm, 1.5 μm, and 100 nm) were prepared by controlling the reaction temperature and time, pH value, amount of reducing agent, and polyvinylpyrrolidone in the reaction system. The Seebeck coefficient, electrical conductivity, and thermal conductivity of the cement composites with 5.0 wt.% nanostructured Cu_2O powder increased to $3966 \pm 54\,\mu$V/K, $(2.68 \pm 0.12) \times 10^{-4}$ S/m, and 0.69 ± 0.007 W/(m·K), respectively. Thereby, a high figure of merit value of 1.93×10^{-6} was obtained for the cement composites, which made future application of cement composites in energy harvesting for buildings possible.

1. Introduction

Buildings consume considerable resources and energy in the process of construction and use. To promote sustainable buildings, energy saving and emission reduction have become the focus of attention in the world [1]. For example, some thermoelectric devices installed in walls are utilized to harvest waste heat or refrigerate buildings naturally [2]. However, it is difficult to promote the application of traditional thermoelectric devices made of Bi_2Te_3, PbTe, SiGe, and other alloys in buildings due to the large size of buildings and high cost of thermoelectric materials [3]. Concrete walls and roofs made of thermoelectric cement-based materials might be a way to solve the above problem. However, due to the low Seebeck coefficient and electrical conductivity, the thermoelectric efficiency of cement-based materials is usually low [4].

Thermoelectric components, such as carbon fibers, carbon nanotubes, steel fibers, graphene, graphite oxide, carbon black, alloys, and metal oxides, are incorporated into cement-based materials to increase their thermoelectric efficiency [4–10]. Conductive materials, including carbon fibers, carbon nanotubes, and steel fibers, can increase the electrical conductivity of cement-based materials significantly, while they cannot increase the Seebeck coefficient of cement-based materials significantly [4, 5, 11]. The low Seebeck coefficient of cement-based materials with conductive materials results in low thermoelectric efficiency. Different methods were carried out to modify the conductive components and increase the Seebeck coefficient of cement-based materials. For example, Wei et al. introduced ionic liquid 1-butyl-3-methylimidazolium bromide on the carbon fiber surface, and increased the Seebeck coefficient of the carbon fiber reinforced concrete to $-250\,\mu$V/K at a 1.2 wt.% content [7]. Jia et al. treated reduced graphene oxide with Cl_2 and HNO_3, and increased the Seebeck coefficient of the cement matrix to $-56.61\,\mu$V/K at a 5 wt.% content [12].

Tzounis et al. doped multiwalled carbon nanotubes with nitrogen, and increased the Seebeck coefficient of the cement matrix to −920 μV/K at a 1 wt.% content [13].

Semiconductive materials usually contribute more to the Seebeck coefficient of cement-based materials than conductive materials, which was mainly caused by the low carrier concentration of semiconductive materials [14]. For example, Liu et al. increased the Seebeck coefficient of carbon fiber reinforced cement composites to 36.3 μV/K by incorporating 0.6 wt.% Bi_2Te_3 [15]. Wei et al. found that when the content of Fe_2O_3 and Bi_2O_3 powder was 5.0 wt.%, the Seebeck coefficient of carbon fiber reinforced concrete reached 92.57 and 100.28 μV/K, respectively [16]. However, semiconductive materials cannot increase the electrical conductivity of cement-based materials significantly, resulting in low thermoelectric efficiency of cement-based materials. One research strategy to solve this problem is increasing the electrical conductivity of cement-based materials by introducing conductive materials [17, 18]. Another research strategy is further increasing the Seebeck coefficient of cement-based materials by modifying the semiconductive materials. For example, Wei et al. doped ZnO with Al, Mg, and Ti atoms, and increased the Seebeck coefficient of the cement matrix to –419 μV/K at a 5 wt.% content [19]. Recently, some researchers found that the Seebeck coefficient of transition metal oxides can be further enhanced when the particle size decreases to the nanoscale [20, 21]. In addition, Ghaharia et al. increased the Seebeck coefficient of cement-based composites dozens of times by adding nanostructured ZnO powder into the cement matrix [10]. It is interesting to see how and to which extent can the particle size of semiconductive materials contribute to the Seebeck coefficient and thermoelectric efficiency of cement-based materials.

Herein, a common p-type semiconductor material, named Cu_2O, was prepared by a hydrothermal method and utilized to increase the thermoelectric effect of the cement matrix. It is expected that the Seebeck coefficient of the cement composites can be significantly increased by decreasing the particle size of added Cu_2O powder. Thermoelectric properties, including Seebeck coefficient, electrical conductivity, and thermal conductivity of the cement composites with Cu_2O powder were tested and discussed in detail.

2. Materials and Methods

2.1. Preparation of Cu_2O Powder and Cement Composites. Copper sulfate pentahydrate ($CuSO_4{\cdot}5H_2O$), glycine ($C_2H_5NO_2$), sodium hydroxide (NaOH), and polyvinylpyrrolidone ($(C_6H_9NO)_n$) with a relative molecular weight of 30,000 were purchased from Sinopharm Chemical Reagent Co., Ltd and utilized to prepare Cu_2O powder without any purification. The Cu_2O powder was synthesized via a hydrothermal method, which was similar to the reported method [22]. An amount of $CuSO_4{\cdot}5H_2O$ (2.50 g) and a certain amount of $C_2H_5NO_2$ were dissolved in 20 mL deionized water and stirred by magnetism for 10 min. A certain amount of polyvinylpyrrolidone (PVP) was dissolved in 20 mL deionized water and stirred by magnetism for 10 min. The PVP solution was added to the $CuSO_4{\cdot}5H_2O$ solution drop by drop under magnetic stirring, and then 10 mL of NaOH solution (2 mol/L) was added to the mixture drop by drop under magnetic stirring. Then the mixture was transferred to an autoclave equipped with a 100 mL polytetrafluoroethylene liner and kept in an oven at 150°C for 6 hours. After the reaction, the product was cooled naturally, centrifuged at a rotating speed of 7000 revolutions/min, and washed with deionized water and ethanol several times. The obtained precipitate was dried in an oven at 60°C for 48 h and collected for further characterization. Different preparation conditions were used to change the crystal structure and particle size of Cu_2O, as shown in Table 1 [23, 24].

Table 1: Synthesis conditions of the Cu_2O samples.

Series	$C_2H_5NO_2$ (g)	Temperature (°C)	NaOH solution (mL)	PVP (g)
C1	0.80	150	10	0
C2	1.30	150	10	0
C3	1.80	150	10	0
C4	1.30	150	10	0.50
C5	1.30	150	10	5.00

Cement, fly ash, water, superplasticizer, and the synthesized Cu_2O powder were utilized to make the cement composites with a good workability, as shown in Table 2 [25, 26]. The Cu_2O powder was added to water and dispersed ultrasonically for 30 minutes to obtain a mixture, which was then mixed with cement by a cement paste mixer [25]. The obtained mixture was cast in a cuboid mold ($40 \times 40 \times 160$ mm) for the Seebeck coefficient and electrical conductivity test, and a cylindrical mold ($\varphi 130 \times 40$ mm) for the thermal conductivity test. The prepared cement composites were placed in a standard curing room for 28 days. Before each test, the specimens were dried at 60°C for 72 hours to remove moisture [25].

2.2. Characterization of the Synthesized Cu_2O Powder. The crystal structure of the Cu_2O powder was characterized by X-ray diffraction (XRD) with a CuKa radiation source. The scanning range of the X-ray diffractometer was 10–80° with a step size of 0.02°. Its operating voltage was 40 kV, and its current was 40 mA. The obtained XRD results were analyzed by MDI Jade 5.0 software. The micromorphology of the Cu_2O powder was characterized by scanning electron microscopy (SEM) at 15 kV. Due to the high surface energy and poor conductivity of the powder, all samples were dispersed in absolute ethanol under sonication and then dripped onto glass slides and sprayed with gold for testing.

2.3. Thermoelectric Properties of the Synthesized Cu_2O Powder and Cement Composites. The Seebeck coefficient of the Cu_2O powder and cement composites was tested by the apparatus shown in Figure 1. One end of the cement paste sample was heated at a rate of 0.05 K/s with a resistance heater, and the other end was kept at room temperature by flowing cold water [26]. The temperature difference between the hot end and cold end was monitored by a pair of K-type

Table 2: Composition of the cement paste mixtures.

Series	Cement (g)	Fly ash (g)	Water (g)	Superplasticizer (g)	Cu_2 O (g)	Cu_2O fraction (%)
M0	300	200	150	3.0	0	0
M1C2/C4/C5	300	200	150	3.0	5	1
M2C2/C4/C5	300	200	150	3.0	10	2
M3C2/C4/C5	300	200	150	3.0	15	3
M4C2/C4/C5	300	200	150	3.0	20	4
M5C2/C4/C5	300	200	150	3.0	25	5

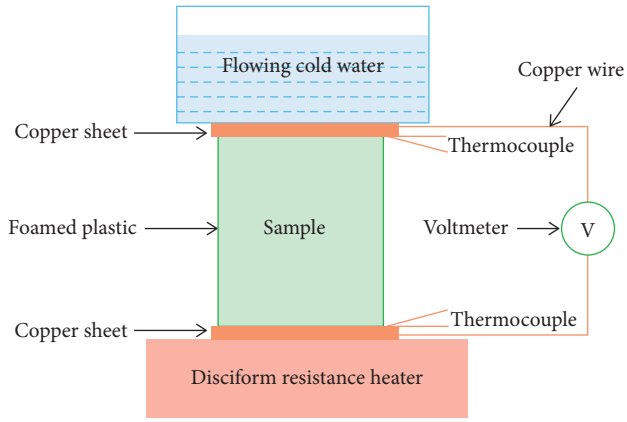

Figure 1: Schematic of the apparatus for the Seebeck coefficient measurement.

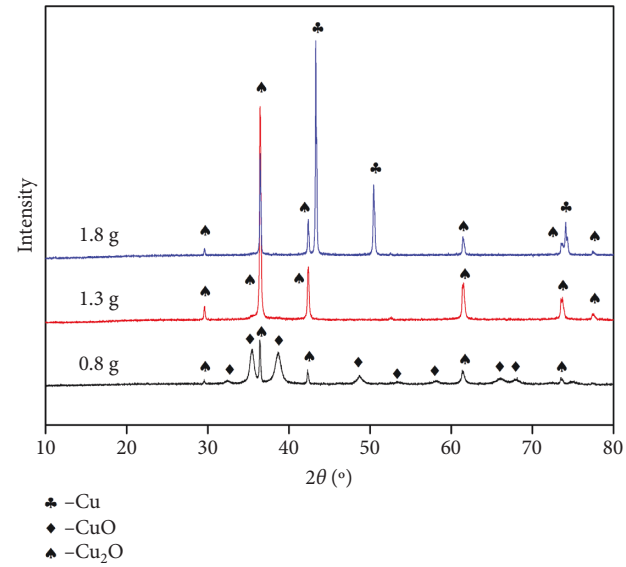

Figure 2: Effect of $C_2H_5NO_2$ dosage on the crystal structure of the reaction products (C1, C2, and C3).

thermocouples, and the generated thermoelectric potential was monitored by a digital multimeter. Thus, dividing the generated thermoelectric potential by the temperature difference can obtain the Seebeck coefficient.

The electrical conductivity of the synthesized Cu_2O powder and cement composites was tested by the typical four-electrode method. The compacted Cu_2O powder was placed in a plastic pipe and pressed to 5 MPa. A direct current output was connected to the external electrodes of the sample. A digital multimeter (Fluke 289 C) connected to the external electrodes was utilized to measure the current flowing through the sample, and another digital multimeter (Fluke 289 C) connected to the inner electrodes was utilized to measure the voltage. Thus, the conductivity can be calculated from the following formula:

$$\sigma = \frac{1}{\rho}, \quad = \frac{IL}{US}, \tag{1}$$

where σ represents the electrical conductivity, ρ represents the resistivity, I represents the current, U represents the voltage, S represents the cross-sectional area of the sample, and L represents the distance between the two inner electrodes.

The thermal conductivity of the cement composites was measured by a tester based on one-dimensional steady-state thermal conduction. A cylindrical cement specimen was placed in the tester with its two bottom sides connected to the hot and cool surface of the tester and the side face connected to the organic insulator. Thus, the thermal conductivity can be calculated from the following formula:

$$\kappa = \frac{I \cdot U \cdot \mathrm{d}}{S \cdot \Delta T}, \tag{2}$$

where κ represents the thermal conductivity of the specimen, I represents the supplied current, U represents the supplied voltage, d represents the thickness of the specimen, S represents the cross-sectional area of the specimen, and ΔT represents the temperature difference between the two sides of the specimen.

3. Results and Discussion

3.1. Characterization and Thermoelectric Properties of the Synthesized Cu_2O Powder. Figure 2 shows the XRD patterns of the products (C1, C2, and C3) prepared with different $C_2H_5NO_2$ dosages and a fixed reaction temperature of 150°C, NaOH solution amount of 10 mL, and reaction time of 6 h. When the amount of $C_2H_5NO_2$ is 0.80 g, the characteristic diffraction peaks of Cu_2O and CuO can be found in the XRD patterns, indicating that the product is a mixture of Cu_2O and CuO under these reaction conditions. When the amount of $C_2H_5NO_2$ increases to 1.30 g, the characteristic diffraction peaks of CuO disappear, indicating that the reaction product is pure Cu_2O. When the amount of $C_2H_5NO_2$

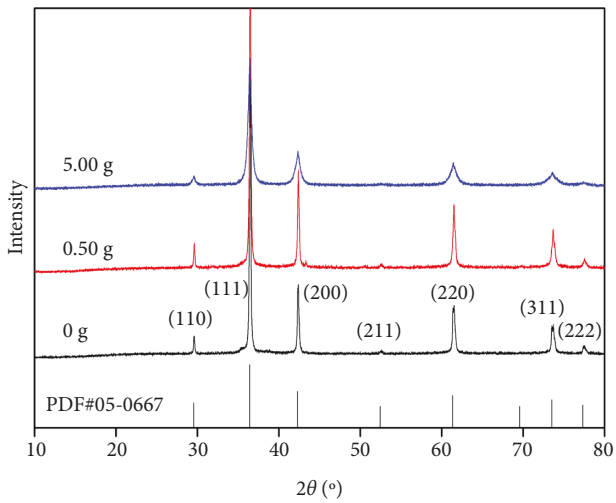

Figure 3: Effect of PVP dosage on the crystal structure of the reaction products (C2, C4, and C5).

increases to 1.80 g, the characteristic diffraction peaks of Cu appear, indicating that the product is a mixture of Cu_2O and Cu. Increasing the amount of $C_2H_5NO_2$ makes the crystal structure of the product change from CuO to Cu_2O, and finally to Cu. Under alkaline conditions, the formation of Cu_2O is preferred due to the larger reducing potential of $Cu(OH)_2/Cu_2O$ compared to $Cu(OH)_2/Cu$ (reactions 3 and 4) [27].

$$Cu(OH)_2 + 2e^- \longrightarrow Cu + 2OH^- \; E^0 = -0.222\,V, \tag{3}$$

$$2Cu(OH)_2 + 2e^- \longrightarrow Cu_2O + 2OH^- + H_2O \quad E^0 = -0.08\,V. \tag{4}$$

Therefore, pure cuprous oxide crystals cannot be obtained in the hydrothermal reaction if the amount of reducing agent is too high or too low.

To prepare cuprous oxide powder with different particle sizes, different amounts of PVP were added to the reaction system. Figure 3 shows the XRD patterns of the samples (C2, C4, and C5) prepared with different dosages of PVP by fixing the reaction temperature of 150°C, the dosage of $C_2H_5NO_2$ of 1.30 g, the dosage of NaOH solution of 10 mL, and the reaction time of 6 h. The diffraction peak positions of the samples prepared with different PVP dosages are the same, and all the samples have characteristic diffraction peaks at 29.56°, 36.42°, 42.30°, 52.45°, 61.34°, 73.52°, and 77.32°. These characteristic diffraction peaks correspond to the diffraction of the Cu_2O crystal faces (110), (111), (200), (211), (220), (311), and (222), according to the PDF card (no. 05–0667). In addition, no other diffraction peaks can be found in the XRD patterns, indicating that PVP does not influence the crystal structure of the reaction product. The PVP in the reaction system, acting as a surfactant, does not influence the redox performance of $C_2H_5NO_2$ [22].

Figure 4 shows the SEM images of the reaction products (C2, C4, and C5) under different dosages of PVP by fixing the reaction temperature of 150°C, the dosage of $C_2H_5NO_2$ of 1.30 g, the dosage of NaOH solution of 10 mL, and the reaction time of 6 h. When the dosage of PVP is 0 g, the cuprous oxide shape is nearly regular octahedra with clear edges and corners. The edge length of the octahedra is approximately 15 μm. The octahedra shape is a characteristic morphology of cuprous oxide according to previous studies [23, 28, 29]. When the amount of PVP increases to 0.50 g, the edges and corners of some cuprous oxide particles are no longer clear, indicating that the growth of crystals is inhibited. The size of these cuprous oxide particles is approximately 1.5 μm. In the solution with a low PVP concentration, PVP covers some faces of cuprous oxide and blocks its further growth [24, 30]. When the dosage of PVP increases to 5.00 g, the growth of cuprous oxide crystals is significantly inhibited. The obtained cuprous oxide shape is nearly spherical with a diameter of approximately 100 nm. The spherical shape is also a characteristic morphology of cuprous oxide according to previous studies [31]. In the solution with high PVP concentration, PVP covers all faces of cuprous oxide, resulting in restricted equiaxial growth [24]. The morphological observation results from SEM are consistent with the test results from XRD. As the growth of the cuprous oxide particles in some directions is restricted by PVP, the intensity of the diffraction peaks decreases with increasing PVP concentration in the reaction.

Figure 5 shows the variation of thermoelectric potential with temperature difference of compacted Cu_2O powder with different particle sizes (C2, C4, and C5) during the heating process from 300 to 350 K. The thermoelectric potential of each Cu_2O sample increases with increasing temperature difference, and their relationship is roughly linear. Thus, the Seebeck coefficients of the compacted Cu_2O powder with different particle sizes can be obtained by linear fitting the relationship between thermoelectric potential and temperature difference, as shown in Table 3. The Seebeck coefficients of C2, C4, and C5 are all positive, indicating that the synthesized Cu_2O is a p-type semiconductor material. The Seebeck coefficient of compacted Cu_2O powder increases gradually with decreasing particle size, and the Seebeck coefficient increases significantly after the particle size enters the nanoscale. The result was similar to that of MnO_2 film, as the Seebeck coefficients of the MnO_2 films with different thicknesses (160, 200, 220, and 250 nm) were 2,500, 2,300, 1,750, and 1,600 $\mu V/k$, respectively [32]. Pichanusakorn gave the Seebeck coefficient calculation formula for thermoelectric materials as follows [33]:

$$S = \mp\frac{1}{eT}\left(\frac{\int_{E_0}^{+\infty} g(E)\tau(E)Ev^2(E)\mathrm{d}f_0/\mathrm{d}E\mathrm{d}E}{\int_{E_0}^{+\infty} g(E)\tau(E)v^2(E)\mathrm{d}f_0/\mathrm{d}E\mathrm{d}E} - E_F\right), \tag{5}$$

where S represents the Seebeck coefficient, e represents the electric charge carried by the electron, T represents the absolute temperature, g(E) represents the simplified electronic density of states of the material, τ(E) represents the electron relaxation time, f_0(E) represents the distribution of the electron, E represents the energy of the electron level, E_0 represents the ground state energy level, and E_F represents the energy of the Fermi level. It can be found that the

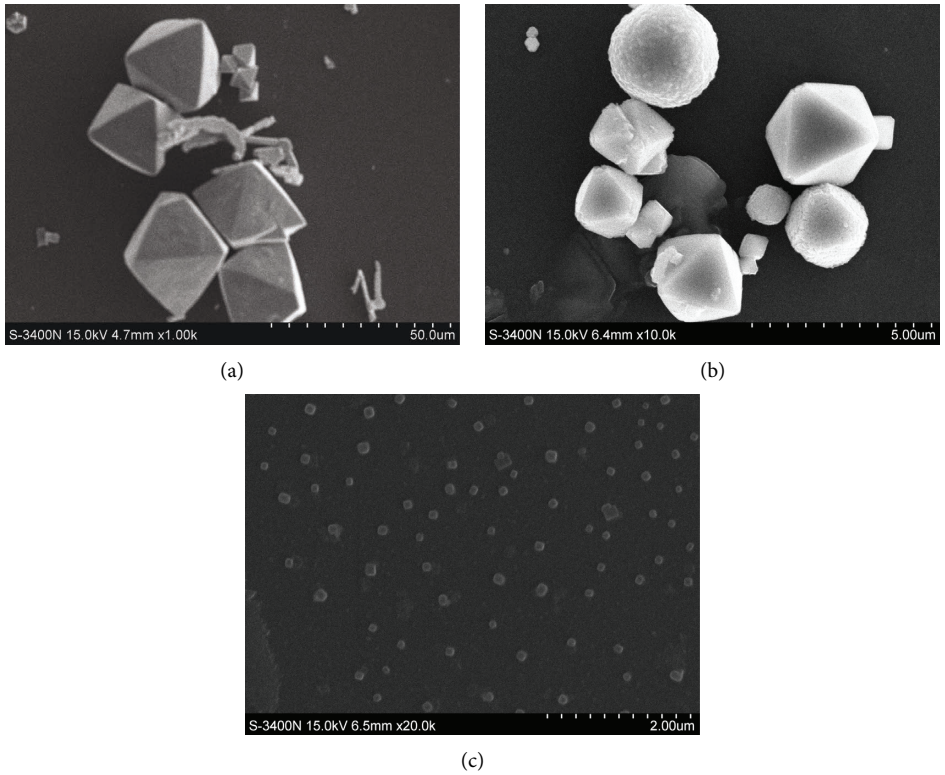

(a) (b)

(c)

Figure 4: SEM images of the Cu_2O particles prepared with different PVP dosages: (a) 0 g, (b) 0.50 g, and (c) 5.00 g.

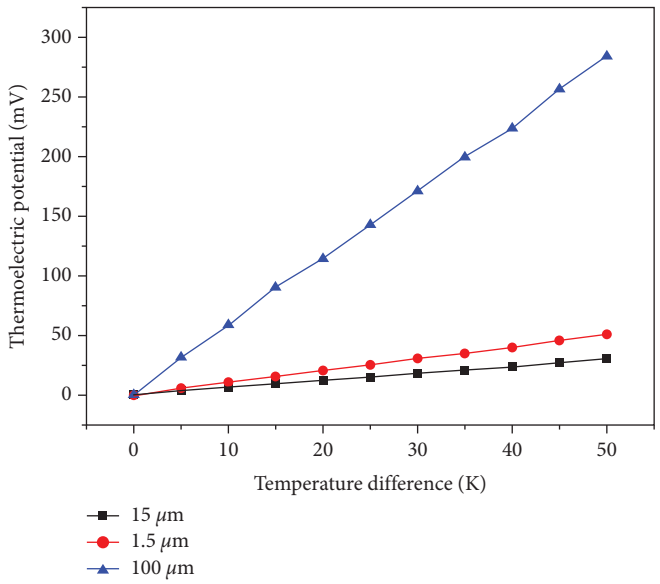

Figure 5: Relationship between the temperature difference and thermoelectric potential of the compacted Cu_2O powders with different particle sizes.

Table 3: Seebeck coefficient and electrical conductivity of the compacted Cu_2O powders with different particle sizes.

Particle size	15 μm	1.5 μm	100 nm
Seebeck coefficient (μV/K)	608 ± 17	1018 ± 26	5708 ± 37
Electrical conductivity (10^{-3} S/m)	1.95 ± 0.03	2.84 ± 0.04	4.55 ± 0.06

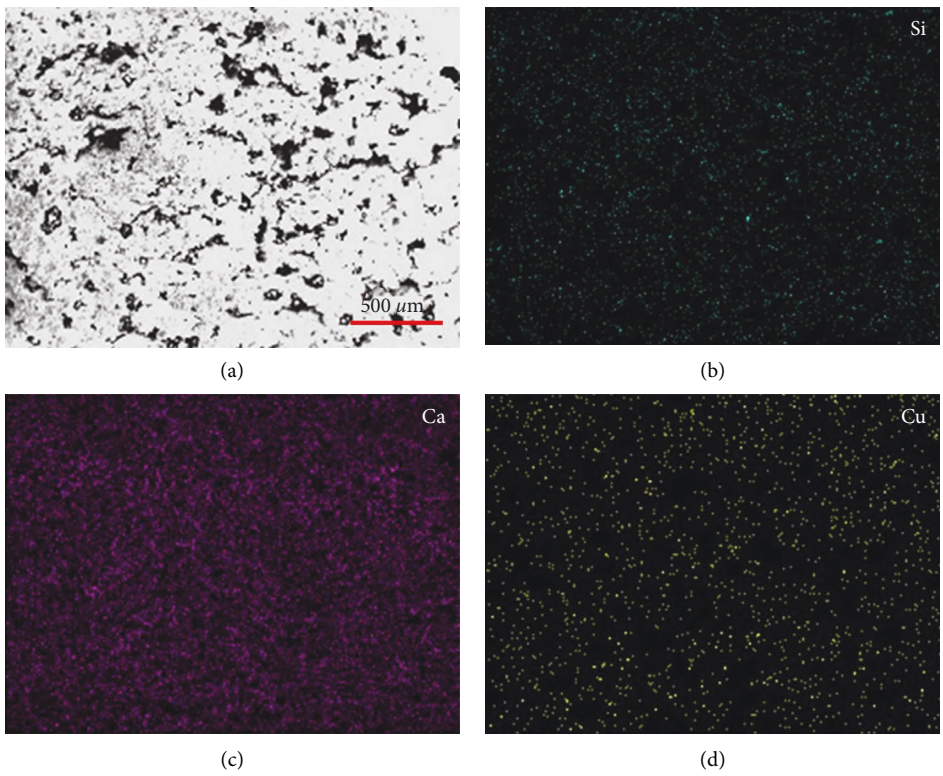

Figure 6: SEM image of the hardened cement composites with (a) 5.0% by weight Cu_2O powder inside, and the elemental mappings of (b) silicon; (c) calcium; and (d) copper.

increase in the density of states near the Fermi level will lead to an increase in the Seebeck coefficient, and the large change in the electronic density of states caused by the quantum confinement effect after materials enter the nanoscale will lead to an obvious difference in the Seebeck coefficient. This explains why the Seebeck coefficient of cuprous oxide powder increases significantly when the size of cuprous oxide is reduced to 100 nm.

The electrical conductivity values of the compacted Cu_2O powders with different particle sizes at 300 K are listed in Table 3. The electrical conductivity increases with decreasing particle size of the Cu_2O powder. This may be caused by the pore size difference in the compacted Cu_2O samples. Since the pore size decreases with decreasing particle size of Cu_2O powder, fast conductive paths for hole transport are formed in compacted Cu_2O powder with small particle size. In fact, the compacted 100 nm Cu_2O particles exhibited a higher electrical conductivity value (4.55×10^{-3} S/m) than the compacted 15 μm Cu_2O particles (1.95×10^{-3} S/m). However, the difference in electrical conductivity of the compacted Cu_2O powder caused by the particle size is less pronounced than that in Seebeck coefficient. Because of the larger Seebeck coefficient and electrical conductivity, the thermoelectric output of compacted nanostructured Cu_2O powder is much higher than that of compacted micro-Cu_2O powder. Then, the prepared Cu_2O powders with different particle sizes were added to the cement matrix to determine the influence on the thermoelectric properties of cement composites. Figure 6 shows the distribution mappings of the main elements in the cement composites. The Cu element distributes across the tested area uniformly, indicating that Cu_2O particles distribute uniformly in the hardened cement composites.

3.2. Thermoelectric Properties of the Cement Composites with Cu_2O Powder. Figure 7 shows the variation of thermoelectric potential with temperature difference of cement composites with added nanostructured Cu_2O powder during the heating process from 300 to 345 K. The thermoelectric potential of the hardened cement paste without Cu_2O powder is close to 0, indicating that the thermoelectric effect of the cement composites mainly relies on the added Cu_2O powder. The thermoelectric potential values of the cement composites with added Cu_2O powder are positive, indicating that the cement composites with added Cu_2O powder exhibit p-type semiconductor properties. This is different from the n-type cement composites with added MnO_2 powder in our previous study [25]. The thermoelectric potential of the cement composites with added nanostructured Cu_2O powder increases with increasing temperature difference. Under the same temperature difference, the thermoelectric potential increases with increasing content of added nanostructured Cu_2O powder. The relationship between the thermoelectric potential and temperature difference is roughly linear, and the slope of the straight line represents the Seebeck coefficient.

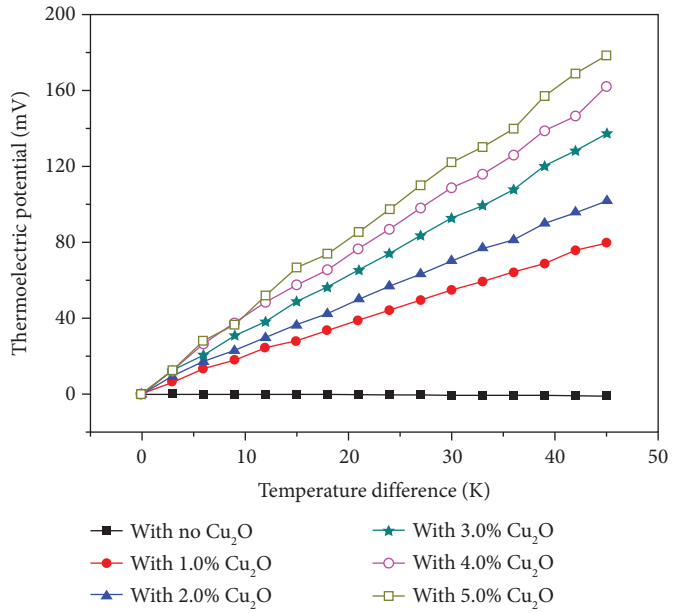

FIGURE 7: Relationship between the temperature difference and thermoelectric potential of cement composites with added nanostructured Cu_2O powder.

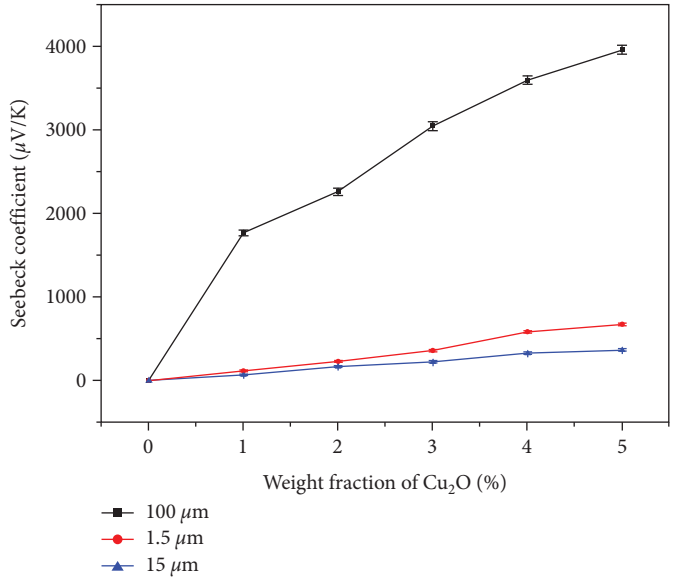

FIGURE 8: Relationship between the Seebeck coefficient of cement composites and weight fraction of added Cu_2O powder with different particle sizes.

The Seebeck coefficients of the prepared cement matrix samples with added Cu_2O powder of different grades were calculated by linear fitting, the relationship between the thermoelectric potential and temperature difference of the cement composites, as shown in Figure 8. The Seebeck coefficient of the cement composites varies with the content and particle size of the added Cu_2O powder. In detail, it increases with increasing content of added Cu_2O powder. When the content of added Cu_2O powder (100 nm, 1.5 μm, and 15 μm) in the cement composites reached 5.0 wt.%, the largest Seebeck coefficient reached 3966, 670 and 364 μV/K, respectively. In addition, when the content of Cu_2O powder is the same, a large Seebeck coefficient of the cement composites can be obtained by decreasing the Cu_2O particle size. For example, the largest Seebeck coefficient of the cement composites with 100 nm Cu_2O powder was approximately 6 times higher than that of cement composites with 1.5 μm Cu_2O particles, and it was 10 times higher than that of cement composites with 15 μm Cu_2O particles. The significantly increased Seebeck coefficient of the cement composites with 5.0 wt.% nanostructured Cu_2O particles was similar to that of cement composites with added nanostructured MnO_2 particles (−3085 μV/K) [25]. This value was far higher than the reported values of cement

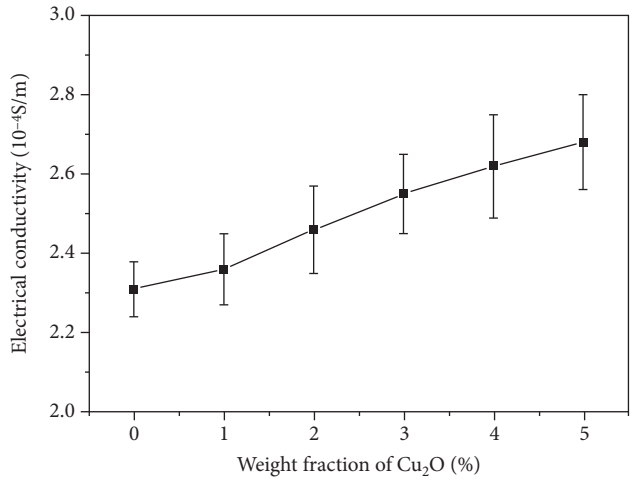

Figure 9: Relationship between the electrical conductivity of cement composites and weight fraction of added nanostructured Cu_2O particles.

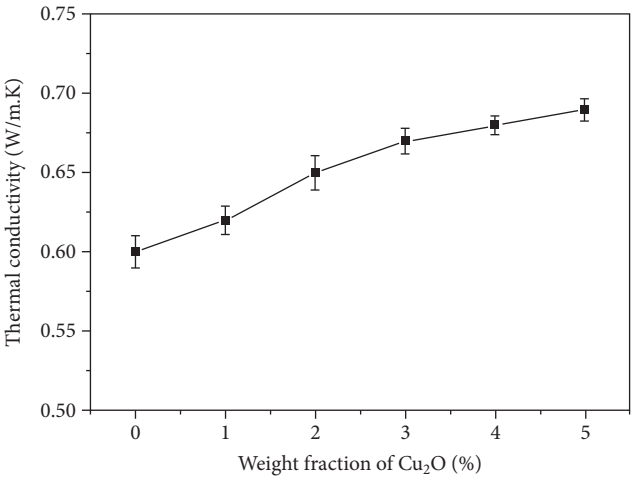

Figure 10: Relationship between the thermal conductivity of cement composites and weight fraction of added nanostructured Cu_2O particles.

composites with added micro Fe_2O_3 (92.57 μV/K) or Bi_2O_3 (100.28 μV/K) [16]. The nanostructured metal oxide particles possess a larger gradient of the density of states near the Fermi energy than the microparticles, causing a sharp increase in the Seebeck coefficient [34]. In addition, the nanostructured metal oxide particles introduced more interfaces in the cement matrix, which is beneficial to the Seebeck coefficient of cement composites [16, 35]. Introducing more nanostructured metal oxide particles may further increase the Seebeck coefficient of cement composites, but it would result in negative effects on setting time, mechanical strength, and deterioration resistance [36, 37].

The variation tendencies of electrical conductivity with content of added Cu_2O of different particle sizes are the same for the hardened cement composites. Figure 9 shows the change in the electrical conductivity of the cement composites with the content of nanostructured Cu_2O particles at 300 K. The electrical conductivity values were in the range of 2.2×10^{-4}–2.6×10^{-4} S/m, indicating that the cement composites with added nanostructured Cu_2O particles were insulating materials. The electrical conductivity of the cement composites with added Cu_2O powder was far less than that of cement composites with conductive components inside (0.64 S/m for expanded graphite, 0.27 S/m for reduced graphene oxide, 0.11 S/m for Bi_2Te_3, and 1.95 S/m for n-type nitrogen-doped CNTs) [11, 13, 15, 38]. There are two main types of conductive carriers in the cement composites: various ions in the pore solution, including K^+, Na^+, Ca^{2+}, OH^-, and SO_4^{2-}, and electrons and holes carried by the hydration products, water, cement particles, and cuprous oxide [39, 40]. Due to the poor electrical conductivity and low content of Cu_2O particles, the carried free holes cannot form a conductive network in the cement matrix, resulting in a limited effect on improving the electrical conductivity of the cement composites.

The variation tendencies of thermal conductivity with the content of added Cu_2O of different particle sizes are the same for the hardened cement composites. Figure 10 shows the change in the thermal conductivity of the cement composites with the content of nanostructured Cu_2O particles at 300 K. The thermal conductivity of the cement composites increases with the increasing content of added nanostructured Cu_2O particles. The obtained maximum thermal conductivity values were 0.63, 0.67, and 0.69 W/(m·K) for the cement composites with 5 wt.% 15 μm, 1.5 μm, and 100 nm Cu_2O particles, respectively. They were 5.0%, 11.7%, and 15.0% higher than that of the hardened cement paste without Cu_2O powder. Although bulk Cu_2O possesses a high thermal conductivity, pores, cracks, and other components increase the phonon transmission path in the cement composites, resulting in a restricted effect on the thermal conductivity of the cement composites [41]. The introduced micro- or nanoparticles can fill the voids between the hydration products, decrease the porosity of the cement composites, and increase the thermal conductivity [10]. These factors were responsible for the increased thermal conductivity of the cement composites after decreasing the size of the added Cu_2O particles.

The thermoelectric efficiency is usually evaluated by the figure of merit (ZT), as shown in the following formula:

$$ZT = \left(\frac{S^2\sigma T}{\kappa}\right), \tag{6}$$

where S, σ, κ, and T represent the Seebeck coefficient, electrical conductivity, thermal conductivity, and absolute temperature, respectively. The calculated ZT values of the cement composites are listed in Table 4. The obtained ZT values were 1.96×10^{-8}, 5.48×10^{-8}, and 1.93×10^{-6} for the cement composites with 5 wt.% 15 μm, 1.5 μm, and 100 nm Cu_2O particles, respectively. For the cement composites with 5 wt.%, 100 nm Cu2O particles possessed the largest value in this work. This value was higher than that of cement composites with some unmodified thermoelectric components, such as carbon fiber (1.609×10^{-7}) and MnO_2 particles (7.596×10^{-7}) [21, 42].

Table 4: The Seebeck coefficient, electrical conductivity, thermal conductivity, and average ZT of different series of cement composites.

Series	Seebeck coefficient (μV/K)	Electrical conductivity (10^{-4} S/m)	Thermal conductivity (W/(m·K))	ZT
M0	-0.3 ± 0.04	2.31 ± 0.07	0.60 ± 0.010	1.09×10^{-14}
M5C2	364 ± 15	2.54 ± 0.11	0.63 ± 0.007	1.96×10^{-8}
M5C4	670 ± 17	2.59 ± 0.10	0.67 ± 0.009	5.48×10^{-8}
M5C5	3966 ± 54	2.68 ± 0.12	0.69 ± 0.007	1.93×10^{-6}

However, the obtained ZT value was lower than that of cement composites with some modified thermoelectric components, such as ZnO/expanded graphite (8.7×10^{-3}) and graphene/ZnO nanoinclusions (1.01×10^{-2}) [19, 43]. The low electrical conductivity of the cement composites with added Cu_2O powder results in a limited increase in ZT. The low ZT value restricts the current application of the cement composites with nano Cu_2O particles in energy harvesting in buildings, considering the low efficiency and economy. But the cement composites with nano Cu_2O particles can be used to monitor the temperature of concrete structures. The composites, such as the ZnO/expanded graphite, graphene/ZnO nanoinclusions, and graphite/MnO_2, can dramatically increase the electrical conductivity and thermoelectric efficiency of the cement composites [43–45]. Based on the received results, we would increase the electrical conductivity of the cement composites with added Cu_2O powder by doping the Cu_2O crystals or compositing the Cu_2O particles with conductive materials in the following work [19, 44]. Thus, the thermoelectric efficiency of the cement composites can be further improved and the application in energy harvesting may come true.

4. Conclusions

We synthesized Cu_2O with different particle sizes based on the redox reaction of $CuSO_4{\cdot}5H_2O$ and $C_2H_5NO_2$ and utilized the Cu_2O powder to increase the thermoelectric properties of the cement composites. Based on the results, the following conclusions can be drawn:

(1) Pure Cu_2O crystals can be prepared by controlling the pH value, reaction temperature and time, and content of redox agents in the reaction system. The Cu_2O particle size decreased with increasing PVP content in the reaction system.

(2) The prepared Cu_2O powders with different particle sizes significantly improved the Seebeck coefficient and slightly improved the electrical conductivity and thermal conductivity of the cement composites. The enhanced thermoelectric efficiency of the cement composites was mainly due to the increased Seebeck coefficient.

(3) Nanostructured Cu_2O powder contributes more to the Seebeck coefficient of the cement composites than the micro Cu_2O powder, which is mainly due to the quantum confinement effect after the material entered the nanoscale.

(4) In light of the significantly increased thermoelectric efficiency, the cement composites with added nanostructured Cu_2O powder can be used to monitor temperature difference of concrete structures, and their application in energy harvesting in buildings becomes possible once the electrical conductivity of the cement composites increases to a certain degree.

Data Availability

The data presented in this study are available on request from the corresponding author.

Conflicts of Interest

No potential conflict of interest was reported by the authors.

Acknowledgments

This work was financially supported by the Science Foundation of Nanjing Institute of Technology (No. YKJ201929), the Natural Science Foundation of the Jiangsu Higher Education Institutions of China (No), and the National Science Foundation of China (No. 51525903, 51808369 and 52078247).

References

[1] H. Liu, J. Li, Y. Sun, Y. Wang, and H. Zhao, "Estimation method of carbon emissions in the embodied phase of low carbon building," *Advances in Civil Engineering*, vol. 2020, pp. 1–9, Article ID 8853536, 2020.

[2] Z. B. Liu, L. Zhang, G. Gong, Y. Luo, and F. Meng, "Experimental study and performance analysis of a solar thermoelectric air conditioner with hot water supply," *Energy and Buildings*, vol. 86, pp. 619–625, 2015.

[3] Z. Liu, L. Zhang, G. Gong, H. Li, and G. Tang, "Review of solar thermoelectric cooling technologies for use in zero energy buildings," *Energy and Buildings*, vol. 102, pp. 207–216, Article ID 207216, 2015.

[4] S. Wen and D. D. L. Chung, "Seebeck effect in carbon fiber-reinforced cement," *Cement and Concrete Research*, vol. 29, no. 12, pp. 1989–1993, 1999.

[5] S. Wen and D. D. L. Chung, "Seebeck effect in steel fiber reinforced cement," *Cement and Concrete Research*, vol. 30, no. 4, pp. 661–664, 2000.

[6] S. Ghosh, S. Harish, K. A. Rocky, M. Ohtaki, and B. B. Saha, "Graphene enhanced thermoelectric properties of cement based composites for building energy harvesting," *Energy and Buildings*, vol. 202, Article ID 109419, 2019.

[7] J. Wei, X. Li, Y. Wang et al., "Record high thermoelectric performance of expanded graphite/carbon fiber cement composites enhanced by ionic liquid 1-butyl-3-methylimidazolium bromide for building energy harvesting," *Journal of Materials Chemistry C*, vol. 9, no. 10, pp. 3682–3691, 2021.

[8] H. Min Park, S. Park, I. J. Shon et al., "Influence of Portland cement and alkali-activated slag binder on the thermoelectric properties of the p-type composites with MWCNT," *Construction and Building Materials*, vol. 292, Article ID 123393, 2021.

[9] J. Wei, Z. Miao, Y. Wang et al., "Boosting power factor of thermoelectric cementitious composites by a unique CNT pretreatment process with low carbon content," *Energy and Buildings*, vol. 254, Article ID 111617, 2022.

[10] S. A. Ghahari, E. Ghafari, and N. Lu, "Effect of ZnO nanoparticles on thermoelectric properties of cement composite for waste heat harvesting," *Construction and Building Materials*, vol. 146, pp. 755–763, 2017.

[11] J. Wei, Z. Jia, Y. Wang et al., "Enhanced thermoelectric performance of low carbon cement-based composites by reduced graphene oxide," *Energy and Buildings*, vol. 250, Article ID 111279, 2021.

[12] Z. Jia, J. Wei, Y. Wang, Y. Jiang, and H. Zhang, "Enhanced thermoelectric properties of cement based composites by Cl_2/HNO_3 pretreatment of graphene," *Fullerenes, Nanotubes, and Carbon Nanostructures*, vol. 29, no. 12, pp. 982–990, 2021.

[13] L. Tzounis, M. Liebscher, R. Fuge, A. Leonhardt, and V. Mechtcherine, "P- and n-type thermoelectric cement composites with CVD grown p- and n-doped carbon nanotubes: demonstration of a structural thermoelectric generator," *Energy and Buildings*, vol. 191, pp. 151–163, 2019.

[14] S. Walia, S. Balendhran, H. Nili et al., "Transition metal oxides – thermoelectric properties," *Progress in Materials Science*, vol. 58, no. 8, pp. 1443–1489, 2013.

[15] X. Liu, G. Liao, and J. Zuo, "Enhanced thermoelectric properties of carbon fiber-reinforced cement composites (CFRCs) utilizing Bi_2Te_3 with three doping methods," *Fullerenes, Nanotubes, and Carbon Nanostructures*, vol. 29, no. 4, pp. 295–303, 2021.

[16] J. Wei, L. Hao, G. He, and C. Yang, "Enhanced thermoelectric effect of carbon fiber reinforced cement composites by metallic oxide/cement interface," *Ceramics International*, vol. 40, no. 6, pp. 8261–8263, 2014.

[17] X. Liu, M. Qu, A. P. T. Nguyen, N. R. Dilley, and K. Yazawa, "Characteristics of new cement-based thermoelectric composites for low-temperature applications," *Construction and Building Materials*, vol. 304, Article ID 124635, 2021.

[18] S. Ghosh, S. Harish, M. Ohtaki, and B. B. Saha, "Thermoelectric figure of merit enhancement in cement composites with graphene and transition metal oxides," *Materials Today Energy*, vol. 18, Article ID 100492, 2020.

[19] J. Wei, Y. Wang, X. Li et al., "Dramatically improved thermoelectric properties by defect engineering in cement-based composites," *ACS Applied Materials & Interfaces*, vol. 13, no. 3, pp. 3919–3929, 2021.

[20] Y. Lan, A. J. Minnich, G. Chen, and Z. Ren, "Enhancement of thermoelectric figure-of merit by a bulk nanostructuring approach," *Advanced Functional Materials*, vol. 20, no. 3, pp. 357–376, 2010.

[21] M. G. Kanatzidis, "Nanostructured thermoelectrics: the new paradigm?" *Chemistry of Materials*, vol. 22, no. 3, pp. 648–659, 2010.

[22] J. Zhu, Y. Wang, X. Wang, X. Yang, and L. Lu, "A convenient method for preparing shape-controlled nanocrystalline Cu_2O in a polyol or water/polyol system," *Powder Technology*, vol. 181, no. 3, pp. 249–254, 2008.

[23] X. Zhang, Y. Xie, F. Xu, X. Liu, and D. Xu, "Shape-controlled synthesis of submicro-sized cuprous oxide octahedra," *Inorganic Chemistry Communications*, vol. 6, no. 11, pp. 1390–1392, 2003.

[24] H. Zhang, X. Ren, and Z. Cui, "Shape-controlled synthesis of Cu_2O nanocrystals assisted by PVP and application as catalyst for synthesis of carbon nanofibers," *Journal of Crystal Growth*, vol. 304, no. 1, pp. 206–210, 2007.

[25] T. Ji, X. Zhang, X. Zhang, Y. Zhang, and W. Li, "Effect of manganese dioxide nanorods on the thermoelectric properties of cement composites," *Journal of Materials in Civil Engineering*, vol. 30, no. 9, Article ID 04018224, 2018.

[26] T. Ji, X. Zhang, and W. H. Li, "Enhanced thermoelectric effect of cement composite by addition of metallic oxide nanopowders for energy harvesting in buildings," *Construction and Building Materials*, vol. 115, pp. 576–581, 2016.

[27] K. Chen and D. Xue, "pH-assisted crystallization of Cu_2O: chemical reactions control the evolution from nanowires to polyhedral," *CrystEngComm*, vol. 14, no. 23, pp. 8068–8075, 2012.

[28] S. J. Chen, X. T. Chen, Z. Xue, L. H. Li, and X. Z. You, "Solvothermal preparation of Cu_2O crystalline particles," *Journal of Crystal Growth*, vol. 246, no. 1-2, pp. 169–175, 2002.

[29] Z. Zhang, J. Sui, L. Zhang, M. Wan, Y. Wei, and L. Yu, "Synthesis of polyaniline with a hollow, octahedral morphology by using a cuprous oxide template," *Advanced Materials*, vol. 17, no. 23, pp. 2854–2857, 2005.

[30] Y. Xu, X. Jiao, and D. Chen, "PEG-assisted preparation of single-crystalline Cu_2O hollow nanocubes," *The Journal of Physical Chemistry C*, vol. 112, no. 43, pp. 16769–16773, 2008.

[31] R. M. Mohamed and E. S. Aazam, "Preparation and characterization of core–shell polyaniline/mesoporous Cu_2O nanocomposites for the photocatalytic oxidation of thiophene," *Applied Catalysis A: General*, vol. 480, pp. 100–107, 2014.

[32] A. K. M. F. u. Islam, R. Islam, and K. A. Khan, "Studies of the thermoelectric effect in semiconducting MnO_2 thin films," *Journal of Materials Science: Materials in Electronics*, vol. 16, no. 4, pp. 203–207, 2005.

[33] P. Pichanusakorn and P. Bandaru, "Nanostructured thermoelectrics," *Materials Science and Engineering: R: Reports*, vol. 67, no. 2–4, pp. 19–63, 2010.

[34] H. Alam and S. Ramakrishna, "A review on the enhancement of figure of merit from bulk to nano-thermoelectric materials," *Nano Energy*, vol. 2, no. 2, pp. 190–212, 2013.

[35] J. Wei, Y. Wang, X. Li et al., "Effect of porosity and crack on the thermoelectric properties of expanded graphite/carbon fiber reinforced cement-based composites," *International Journal of Energy Research*, vol. 44, no. 8, pp. 6885–6893, 2020.

[36] M. Kumar, M. Bansal, and R. Garg, "An overview of beneficiary aspects of zinc oxide nanoparticles on performance of cement composites," *Materials Today Proceedings*, vol. 43, pp. 892–898, 2021.

[37] H. Ş. Arel and B. S. Thomas, "The effects of nano-and microparticle additives on the durability and mechanical properties of mortars exposed to internal and external sulfate attacks," *Results in Physics*, vol. 7, pp. 843–851, 2017.

[38] J. Wei, L. Zhao, Q. Zhang, Z. B. Nie, and L. Hao, "Enhanced thermoelectric properties of cement-based composites with expanded graphite for climate adaptation and large-scale energy harvesting," *Energy and Buildings*, vol. 159, pp. 66–74, 2018.

[39] B. Chen, K. Wu, and W. Yao, "Conductivity of carbon fiber reinforced cement-based composites," *Cement and Concrete Composites*, vol. 26, no. 4, pp. 291–297, 2004.

[40] D. D. L. Chung, "Electrically conductive cement-based materials," *Advances in Cement Research*, vol. 16, no. 4, pp. 167–176, 2004.

[41] R. B. Arroyo, "Synthesis of copper oxide aided by selective corrosion in Cu foils," *Advances in Materials Science and Engineering*, vol. 2018, pp. 1–7, Article ID 4231571, 2018.

[42] J. Wei, Z. Nie, G. He, L. Hao, L. Zhao, and Q. Zhang, "Energy harvesting from solar irradiation in cities using the thermoelectric behavior of carbon fiber reinforced cement composites," *RSC Adv.*, vol. 4, no. 89, pp. 48128–48134, 2014.

[43] S. Ghosh, S. Harish, M. Ohtaki, and B. B. Saha, "Enhanced figure of merit of cement composites with graphene and ZnO nanoinclusions for efficient energy harvesting in buildings," *Energy*, vol. 198, Article ID 117396, 2020.

[44] A. N. Grace, S. Y. Choi, M. Vinoba et al., "Electrochemical reduction of carbon dioxide at low overpotential on a polyaniline/Cu_2O nanocomposite based electrode," *Applied Energy*, vol. 120, pp. 85–94, 2014.

[45] X. Liu, M. Qu, and A. P. T. Nguyen, "Characteristics of graphite and MnO_2 enhanced cement-based thermoelectric composite for low-temperature applications," *International High Performance Buildings Conference*, vol. 356, 2021.